



Binder-less and free-standing Co–Fe metal nanoparticles-decorated PVdF-HFP nanofiber membrane as an electrochemical probe for enzyme-less glucose sensors

J. Saravanan¹ · A. Vignesh¹ · Syed Shaheen Shah² · Md. Abdul Aziz² · Mehboobali Pannipara³ · Abdullah G. Al-Sehemi³ · Siew-Moi Phang^{4,5} · Fong-Lee Ng⁴ · Bakrudeen Ali Ahmed Abdul⁶ · G. Gnana kumar¹ 

Received: 2 June 2021 / Accepted: 19 July 2021 / Published online: 19 August 2021
© The Author(s), under exclusive licence to Springer Nature B.V. 2021

Abstract

Co–Fe bimetallic nanoparticles-affixed polyvinylidene fluoride-co-hexafluoropropylene (PVdF-HFP) nanofiber membrane is fabricated using the electrospinning and chemical reduction techniques. The semicrystalline polymeric backbone decorated with the highly crystalline Co–Fe bimetallic nanoparticles enunciates the mechanical integrity, while the incessant and swift electron mobility is articulated with the consistent dissemination of bimetallic nanoparticles on the intersected and multi-layered polymeric nanofibers. The diffusion and adsorption of glucose are expedited in the extended cavities and porosities of as-formulated polymeric nanofibers, maximizing the glucose utilization efficacy, while the uniformly implanted Co⁴⁺/Fe³⁺ active centers on PVdF-HFP nanofibers maximize the electrocatalytic activity toward glucose oxidation under alkaline regimes. Thus, the combinative sorts including nanofiber and nanocomposite strategies of PVdF-HFP/Co–Fe membrane assimilate the enzyme-less electrochemical glucose detection concerts of high sensitivity (375.01 $\mu\text{A mM}^{-1} \text{cm}^{-2}$), low limit of detection (0.65 μM), and wide linear range (0.001 to 8 mM), outfitting the erstwhile enzyme-less glucose detection reports. Additionally, the endowments of high selectivity and real sample glucose-sensing analyses of PVdF-HFP/Co–Fe along with the binder-less and free-standing characteristics construct the state-of-the-art paradigm for the evolution of affordable enzyme-less electrochemical glucose sensors.

Keywords Nanofibers · Bimetallic nanoparticles · Selectivity · Electroactive centers · Utilization rate

✉ G. Gnana kumar
kumarg2006@gmail.com

Extended author information available on the last page of the article

Introduction

Globally, the diabetes mellitus, an assemblage of metabolic disorder, provokes discomforts for 200 million people and an inappropriate treatment of above disease eventually leads to death [1]. In this line, an accurate assessment of anatomical glucose concentration is prudent to prescribe an effective handling of diabetic emergencies such as hyperglycemia (> 7 mM) and hypoglycemia (< 3 mM) [2]. Accordingly, an ascending demand on the progression of sensitive and selective glucose sensors has become the perplexing concern of this hour. Enzyme-less electrochemical glucose sensor (ELEGs) is considered as an intriguing technique to discourse the above-mentioned challenges with the cost- and time-efficient glucose-sensing features [3].

The realization of ELEGs in real-time glucose diagnosis is intensely reliant upon the electrode/electrolyte interfacial properties. Accordingly, a number of electrodes including glassy carbon electrode (GCE) [4], fluorine-doped [5] and indium-doped tin oxides [6], platinum [7], gold [8], and carbonaceous assortments [9] were employed in ELEGs and the alteration of above electrodes' surfaces with catalytic architectures is indispensable because of their lack in the electrically conductive and catalytically active sites. However, the restraints associated with their surface alteration processes including irksome slurry preparation, placement of catalysts on electrode's surface, and an enrollment of an insulating binder pull a back to the evolution of ELEGs [10–12], necessitating the innovative electro-architectures with catalytically active system [13–16].

Owing to the captivating architecture and electrical and mechanical properties, polymeric nanofiber membranes have acclaimed prodigious responsiveness as electrochemical probes in ELEGs. The protracted porosity perceived among the nanofibers and their large surface area accelerate the analyte adsorption efficacy, benefitting their electrochemical supremacies [17]. Generally, the mass production of nanofibers is enunciated with an electrospinning technique; however, the fine-tuning of nanofiber membranes with free-standing and electron conductive characteristics is a monotonous process. Amid the polymers exploited for the fabrication of membranes, PVdF-HFP has enunciated its wide utilization owing to its high dielectric constant, semicrystalline behavior, elevated thermal, mechanical, oxidative, and hydrolytic stabilities, and hydrophobic tendencies [18, 19]

However, their non-catalytic and insulating features obstruct their engagement in ELEGs, which would be astounded with the establishment of metallic active sites. Within a series of metal nanostructures used in ELEGs, cobalt (Co) nanoparticles have been acclaimed because of the beneficial features including large specific surface area, rational electrical conductivity (0.364 S m^{-1}), loftier catalytic activity, and anti-surface poisoning properties [20]. In this line, Tong et al. fabricated the ELEGs with Co nanoparticles-loaded indium tin oxide and scrutinized the detection limit and linear range, respectively, of $0.25 \text{ }\mu\text{M}$ and 0.005 to 0.18 mM [21]. On the other side, Co-modified pillared clay established the coherent sensitivity ($71.96 \text{ }\mu\text{A mM}^{-1} \text{ cm}^{-2}$), detection limit ($4.22 \text{ }\mu\text{M}$), and linear range ($2\text{--}10 \text{ mM}$) on glucose detection [22]. The scrutinized rational electrochemical

sensing performances of Co nanoparticles are accredited with their surface instabilities in an aqueous medium and an improper interaction with an analyte, which could be improved, viz. its bimetallic formation of Co with Fe [23]. However, the lack of substantial glucose oxidation research efforts on Co–Fe nanoparticles not only confines their factual pertinence in ELEGs but also lessens the scale-up evolutions of ELEGs. Accordingly, we develop the Co nanoparticles-assimilated PVdF-HFP nanofiber membrane for the evolution of sensitive and selective ELEGs and its contests in effectual glucose detection are embarked with the bimetallic Co–Fe nanoparticles.

Experimental section

Materials

PVdF-HFP ($MW = 400\,000\text{ g mol}^{-1}$), N,N-dimethylformamide (DMF, AR, 97%), acetone (AR, 99.5%), cobalt (II) chloride (CoCl_2 , AR, $\geq 98\%$), iron (III) chloride (FeCl_3 , AR, 97%), hydrazine monohydrate ($\text{N}_2\text{H}_4 \cdot \text{H}_2\text{O}$, AR, $\geq 97\%$), and other processed interferences were redeemed from Sigma-Aldrich and convened without any refining processes.

Preparation of PVdF-HFP/ Co^{2+} / Fe^{3+} solution

0.15 M CoCl_2 and 0.15 M FeCl_3 were supplemented with 10 wt % PVdF-HFP in DMF/acetone (7:3 v/v) under mild stirring for 1 h at 60 °C.

For a comparison, PVdF-HFP/ Co^{2+} and PVdF-HFP/ Fe^{3+} solutions were prepared by assorting, respectively, the 0.3 M $\text{CoCl}_2 \cdot 6\text{H}_2\text{O}$ and 0.3 M FeCl_3 with 10 wt % PVdF-HFP under indistinguishable regimes from the above.

Electrospinning process

The as-formulated PVdF-HFP or PVdF-HFP/ Co^{2+} or PVdF-HFP/ Fe^{3+} or PVdF-HFP/ Co^{2+} / Fe^{3+} solution was encumbered in a syringe comprising of a stainless steel needle. A power supply of 20 kV was provided to the needle, and a stream rate of 0.3 mL h^{-1} was tuned by a micropump. The drum collector covered by an aluminum foil was rotated at 1500 rpm, and the distance preserved between the needle and drum collector was 13 cm. The subsequent polymeric solution was deposited over the rotating drum collector, and the prevailing solvent molecules in nanofiber membrane were detached at 100 °C.

Preparation of nanostructures-decorated nanofiber membranes

The as-formulated PVdF-HFP or PVdF-HFP/ Co^{2+} or PVdF-HFP/ Fe^{3+} or PVdF-HFP/ Co^{2+} / Fe^{3+} membrane was actuated in 0.1 M $\text{N}_2\text{H}_4 \cdot \text{H}_2\text{O}$ for the formulation of PVdF-HFP or PVdF-HFP/Co or PVdF-HFP/Fe or PVdF-HFP/Co–Fe membrane.

Characterizations

The as-formulated membrane series' structural and morphological traits were studied using the TESCAN-LYRA3-FIB scanning electron microscopy (SEM), D8 Advance ECO X-ray powder diffractometer (XRD), IR Tracer 100 ASCII Fourier transform infrared (FTIR) spectroscopy, and ULVAC-PHI X-ray photoelectron spectroscopy (XPS) techniques.

Electrochemical Characterizations

A routine three-electrode cell assembly made up of working (PVdF-HFP/PVdF-HFP-based nanocomposite membrane), reference (Ag/AgCl), and counter electrodes (Pt wire) was applied to scrutinizing the electrochemical glucose-sensing performances of as-formulated materials using cyclic voltammetry and amperometric techniques.

Results and discussion

Morphological studies

The multi-layered and interlinked fibers with a mean diameter of ~ 280 nm are scrutinized for as-electrospun PVdF-HFP membrane, and the interlaced and sequentially layered fibers enunciate an adequate physical integrity to the relevant fiber membrane [24]. PVdF-HFP/Co exhibits the consistently distributed Co nanoparticles on PVdF-HFP fibers (Fig. 1a). Co^{2+} ions assimilated on PVdF-HFP nanofibers are reduced into Co nanoparticles using the reducing agent of $\text{N}_2\text{H}_4 \cdot \text{H}_2\text{O}$, and the mean diameter of Co nanoparticles decorated on PVdF-HFP fibers is estimated as ~ 198 nm. Moreover, the polymeric fiber diameter of PVdF-HFP/Co membrane is reduced into ~ 230 nm because of the promoted electrical conductivity of PVdF-HFP/Co $^{2+}$ solution via the charged metallic ions (Fig. 1b). On the other side, Co-Fe nanoparticles with an average diameter of ~ 196 nm are unvaryingly spread over the polymeric fibers for PVdF-HFP/Co-Fe membrane (Fig. 1c and d). The prevailing amount of metal nanoparticles on PVdF-HFP nanofibers was scrutinized using the inductively coupled plasma atomic emission spectroscopy (ICP-AES). The contents of Co and Co-Fe on PVdF-HFP nanofibers are established, respectively, as 79 and $(43 + 39) \mu\text{g cm}^{-2}$. The accrued ICP-AES result of PVdF-HFP/Co-Fe is line with the 1:1 ratio of Co and Fe sustained in the formulation of the above polymeric nanocomposite membrane.

Diffraction patterns

As-electrospun PVdF-HFP membrane manifests the distinctive reflection planes including (100), (020), and (021), respectively, at $2\theta = 18.2$, 20, and $38\text{--}40^\circ$ (Fig. 2a), exposing the semicrystalline structure [25]. Together with the distinctive

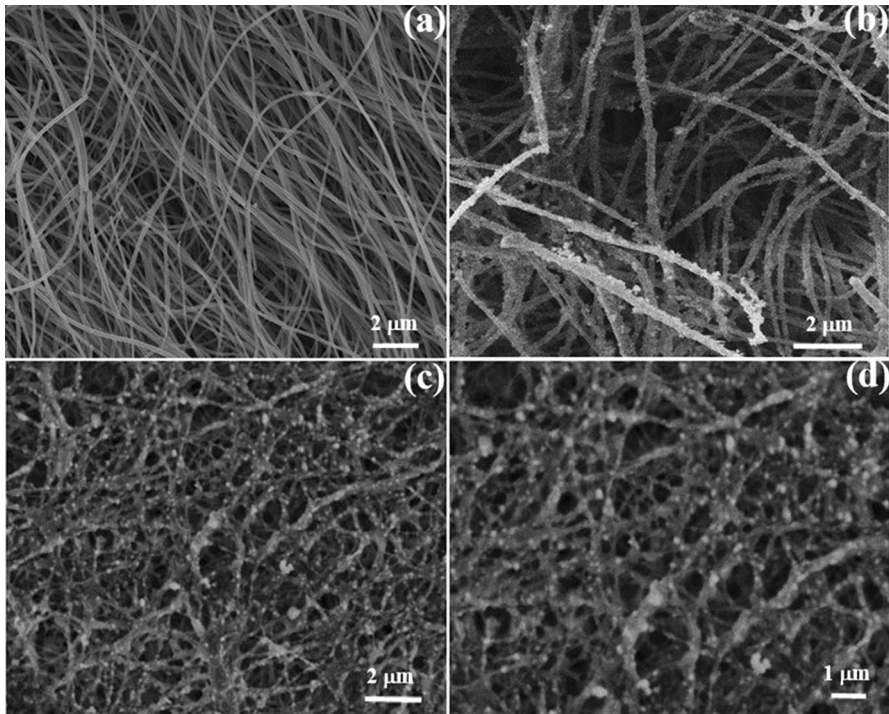
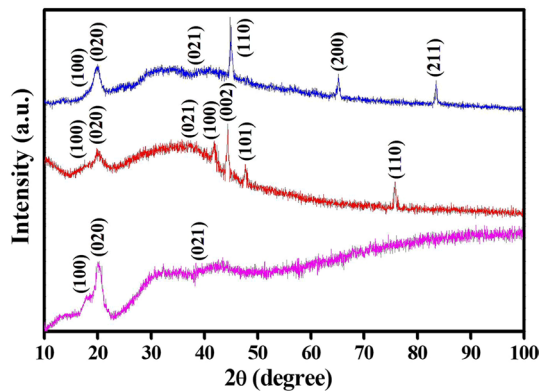


Fig. 1 SEM images of **a** PVdF-HFP, **b** PVdF-HFP/Co, and **c** and **d** PVdF-HFP/Co-Fe membranes

Fig. 2 Diffraction patterns of (—) PVdF-HFP, (—) PVdF-HFP/Co, and (—) PVdF-HFP/Co-Fe membranes



PVdF-HFP planes, the supplemental diffraction peaks pertained with Co are accrued at 41.8, 44.3, 47.80, and 75.82° for PVdF-HFP/Co, epitomizing the reflection planes of (100), (002), (101), and (110), respectively, which itemizes the hexagonal close-packed (hcp) structure (JCPDS No. 05-0727) (Fig. 2b) [26]. On the other side, PVdF-HFP/Co-Fe membrane shows the peculiar diffraction patterns at 45.1, 65.2, and 83.3°, symbolizing the (110), (200), and (211) reflection planes, respectively, of body-centered cubic (bcc) crystalline structure of Fe membrane (JCPDS No.

49–1568) (Fig. 2c and Fig. S1), which enumerates the constitutional prevalence of PVdF-HFP/Co/Fe [27].

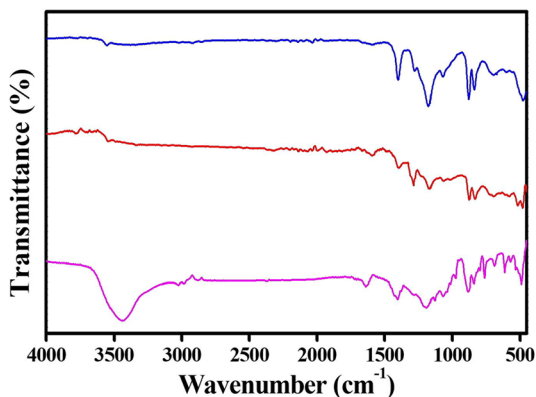
FTIR analysis

The distinctive FTIR peaks of PVdF-HFP electrospun membrane including asymmetric $-\text{CH}_2$ stretching vibrations, deformed vibration of the $-\text{CH}_2$ groups, and symmetric and asymmetric $-\text{CF}_2$ stretching vibrations are inspected, respectively, at 2930, 1405, and 1210 and 1070 cm^{-1} (Fig. 3a) [28]. Together with the above PVdF-HFP's bands, PVdF-HFP/Co establishes the Co–O stretching vibration at 1285 cm^{-1} (Fig. 3b) [29]. The distinctive Fe–O stretching vibration is scrutinized at 672 cm^{-1} [30] for PVdF-HFP/Co–Fe along with the marginally shifted Co–O stretching vibrations, interpreting the formation of PVdF-HFP/bimetallic nanocomposite membrane (Fig. 3c).

XPS studies

The distinctive C, F, Co, and Fe elements scrutinized from the XPS survey scan spectrum disclose the configuration of PVdF-HFP/Co–Fe membrane (Fig. 4a). The distinguishing $-\text{CH}_2$ and $-\text{CF}_2$ units of host polymer in the as-formulated PVdF-HFP/Co–Fe membrane are perceived, respectively, at 286.4 and 290.8 eV in the C 1s core-level spectrum, and the peak at 293.5 eV stipulates the $-\text{CF}_3$ species (Fig. 4b) [18]. The high-resolution F 1s XPS spectrum establishes the covalent and semi-ionic C–F bonds, respectively, at 686.9 and 686.2 eV (Fig. 4c) [18]. The core-level Co 2P spectrum indulges the zero-oxidation state of Co nanoparticles at 778.2 and 792.7 eV, related to the binding energies of Co 2P_{3/2} and Co 2P_{1/2}, respectively. Moreover, the surface oxidized peaks together with their satellite peaks are also witnessed on the core Co 2P spectrum (Fig. 4d) [31]. The pervasiveness of Fe⁰ in PVdF-HFP/Co–Fe membrane is witnessed at 707.0 eV, and the surface-oxidized Fe states are also scrutinized (Fig. 4e) [32].

Fig. 3 FTIR spectra of (—) PVdF-HFP, (—) PVdF-HFP/Co, and (—) PVdF-HFP/Co–Fe membranes



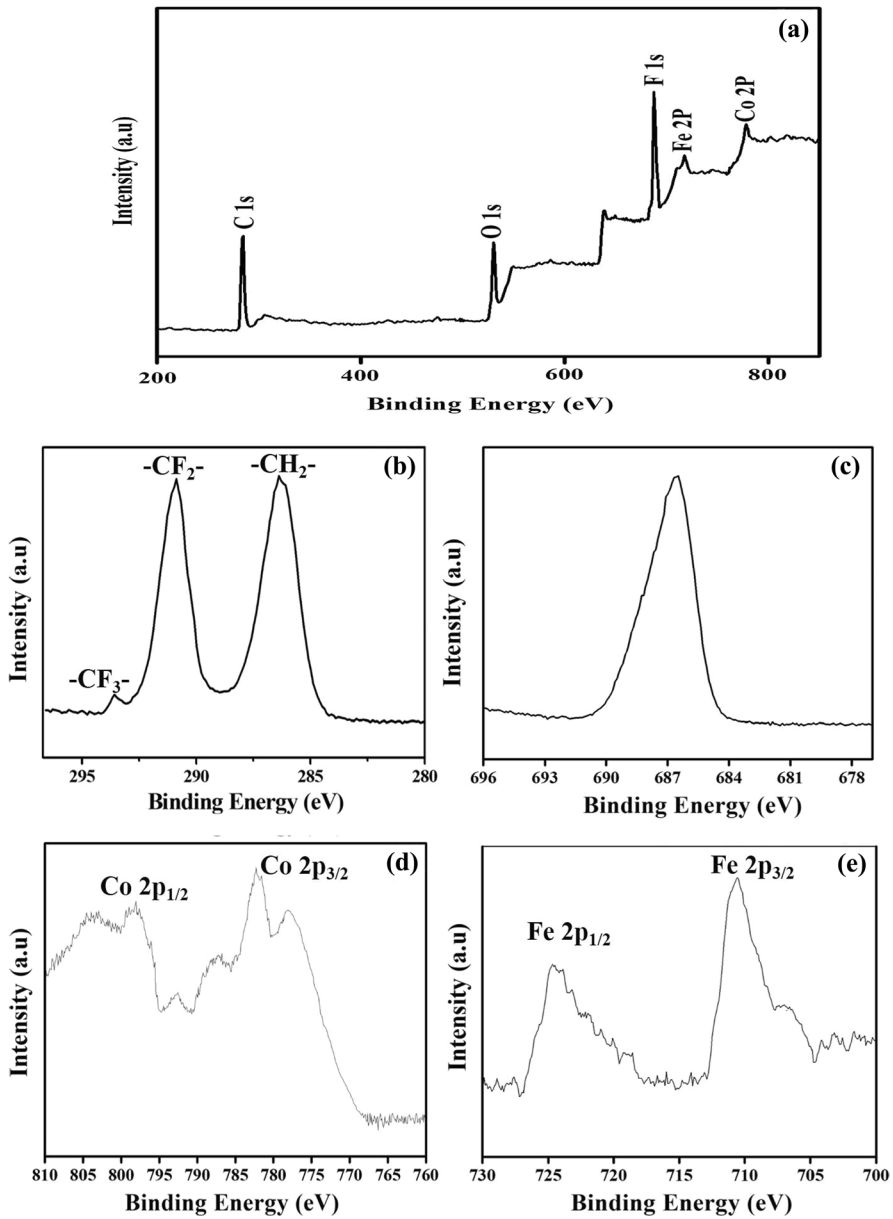


Fig. 4 PVdF-HFP/Co-Fe membrane's **a** wide-scan XPS spectrum and core-level spectra of **b** C 1 s, **c** F 1 s, **d** Co 2p, and **e** Fe 2p

Electrochemical characterizations

The electroactiveness of as-formulated PVdF-HFP membranes was assessed using cyclic voltammetry (CV) in 0.1 M NaOH (Fig. 5a). With the deficiency

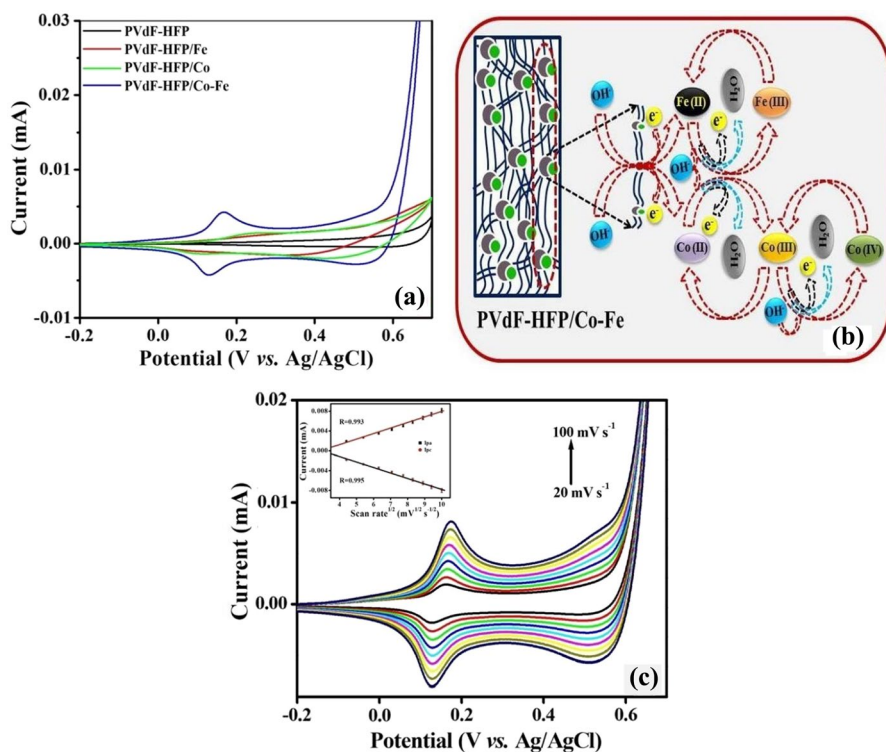


Fig. 5 **a** CVs of as-formulated PVdF-HFPs in 0.1 M NaOH (pH—13) at 50 mV s^{-1} , **b** electrochemical mechanism convoluted at PVdF-HFP/Co-Fe in alkaline regimes, and **c** sweep rate test of PVdF-HFP/Co-Fe (pH—13) (inset: calibration plot of I_{pa}/I_{pc} vs. sweep rate $^{1/2}$)

of electroactive sites, PVdF-HFP membrane does not articulate the electroactive behavior under alkaline regimes. However, the annexation of metallic sites in insulating nanofibers in the form of PVdF-HFP/ monometallic and bimetallic nanocomposites stimulates consequential electroactiveness as manifested from their redox behaviors. PVdF-HFP/Co and PVdF-HFP/Fe expose the perceptible redox couples, representing, respectively, the Co(IV)/Co(III) and Fe(III)/Fe(II) active centers (Fig. 5b). The bimetallic formation of Co with Fe significantly shifts the redox couple to 0.17/0.13 V vs. Ag/AgCl together with the enhanced redox current for the sake of bimetallic synergism [33]. The physisorbed OH^- ions on Co-Fe nanoparticles primarily transform their Co(0)/Fe(0) oxidation states into Co(II)/Fe(II), and the consequent electrochemical oxidation engenders the Co(III)/Fe(III), in which Co(III) is additionally oxidized into Co(IV).

The diffusion-governed progression of PVdF-HFP/Co-Fe in tested electrochemical reaction is scrutinized by witnessing the linear fit between the square root of sweep rate and oxidation (I_{pa}) and reduction peak currents (I_{pc}) (Fig. 5c).

The appraisal of electrocatalytic activities of as-formulated membranes was studied with CV tests upon the instillation of 5 mM glucose (pH—13) (Fig. 6a).

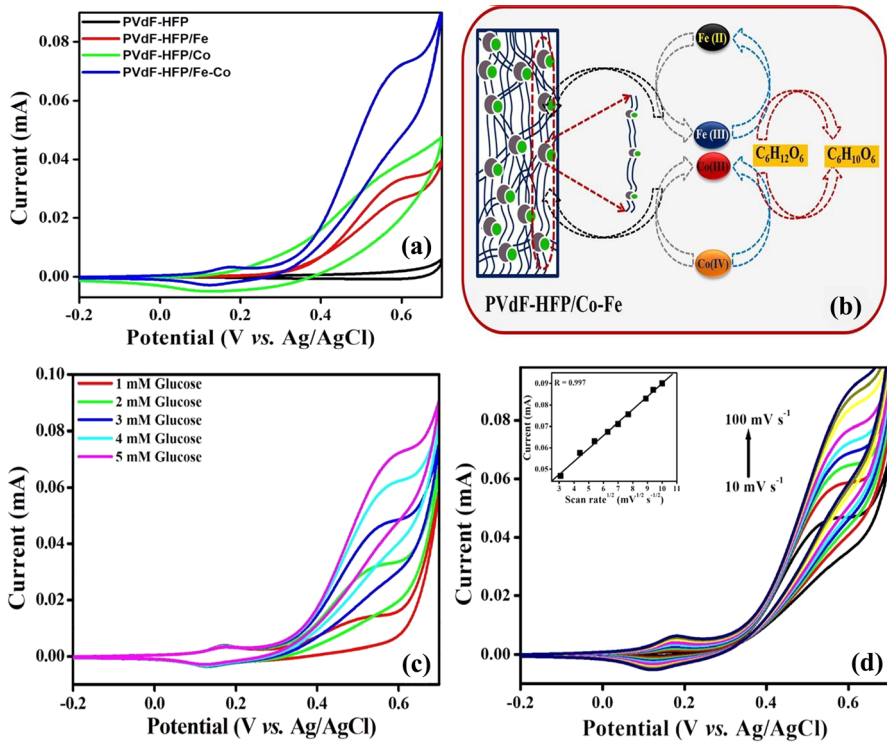


Fig. 6 **a** CVs as-formulated PVdF-HFPs in 5 mM glucose (pH=13) at 50 mV s^{-1} , **b** mechanism convoluted in glucose electrooxidation at PVdF-HFP/Co-Fe, **c** CVs of PVdF-HFP/Co-Fe against dissimilar glucose levels at 50 mV s^{-1} , and **d** sweep rate test of PVdF-HFP/Co-Fe in 5 mM glucose (inset: calibration plot of I_{pa} vs. sweep rate^{1/2})

The electrochemical inertness and insulating nature of PVdF-HFP do not afford any concordant glucose electrooxidation, illuminating the background current. Conversely, PVdF-HFP/Co electrooxidizes glucose at 0.53 V versus Ag/AgCl as conscious from the broad oxidation wave and the Co(III)/Co(IV) active centers generated at PVdF-HFP/Co under alkaline regime rationally electrooxidize the glucose. Despite the concordant glucose oxidation profile scrutinized for PVdF-HFP/Fe, the relevant I_{pa} is inferior to the PVdF-HFP/Co membrane, exposing the confined electrocatalytically active behavior of 'Fe' over the 'Co' nanoparticles on glucose oxidation [33].

The electrooxidation of glucose is additionally endorsed at PVdF-HFP/Co-Fe, and the metal centers of Co(IV)/Fe(III) stimulated under NaOH accelerate the glucose electrooxidation with the supreme oxidation peak current (I_{pa}) of 0.072 mA at 0.60 V versus Ag/AgCl. The protracted voids and ordered porous architectures of nanofibers together with the elevated surface-to-volume ratio endorse the diffusion and adsorption of glucose and commendably store the analyte in PVdF-HFP's reservoirs [34], endorsing the glucose accessibility. The intertwined nanofibers not

only establish the sizeable physical integrity to the PVdF-HFP/Co–Fe membrane, but also administer the swift and incessant electron transference [35]. The prevalence of Co(IV) and Fe(III) centers in Co–Fe mutually escalates the copious reactive and electron mobility channels in PVdF-HFP/Co–Fe. Moreover, the Co–Fe nanoparticles directly grown on polymeric fibers curtail the electron conveyance paths between the current collector and electrochemically active channels and escalate the straight and supreme exposure of glucose with the catalytic centers [36–38]. It augments the electrolyte/electrode interfacial contact area of PVdF-HFP/Co–Fe because of the extended glucose utilization efficacy with the active centers. The exposed Co(IV)/Fe(III) sites of PVdF-HFP/Co–Fe together with the aforementioned productive features efficaciously oxidize glucose, and the appropriate mechanism is delineated in Fig. 6b. The ideal ratio of Co and Fe on effectual glucose oxidation is inspected with the disparity of their contents in as-formulated PVdF-HFP/Co–Fe membrane. The partial replacement of Fe in Co lattices with an equal proportion endorses resistive characteristic against CO/CO₂ poisoning [39], escalating the electrocatalytic activity of PVdF-HFP/Co–Fe(1:1) membrane toward glucose oxidation. However, the increased proportions of Co and Fe in PVdF-HFP/Co–Fe(2:1) and PVdF-HFP/Co–Fe(1:2) nanofiber membranes may generate exorbitant OH_{ads}, which directs the incompetent accessibility of glucose, consequencing an inferior glucose oxidation. Thus, the perceived I_{pa} s in CVs noticeably postulate that 1:1 is a prime ratio for competent ELEGS performance of as-formulated PVdF-HFP/Co–Fe membrane (Fig. S4).

CVs scrutinized for PVdF-HFP/Co–Fe in diversified analyte concentration in 0.1 M NaOH at 50 mV s⁻¹ are portrayed in Fig. 6c. An intensifying concentration of glucose progressively indorses the I_{pa} s, directing the authentic glucose detection process via the amperometric *i*–*t* curves because of the declination in the surface fouling consequences.

The enlisted glucose oxidation electrokinetics at PVdF-HFP/Co–Fe was surveyed with respective of sweep rates in 5 mM glucose (pH=13) (Fig. 6d). I_{pa} s are lifted with an upsurge in the sweep rate, and the linear scale pronounces the diffusion-organized progression.

Amperometric *i*–*t* behavior of PVdF-HFP/Co–Fe membrane

The decisive propriety of PVdF-HFP/Co–Fe on glucose detection was validated using the amperometric *i*–*t* traits against the dissimilar glucose levels (pH=13) at 0.5 V versus Ag/AgCl. A succeeding instillation of an analyte in the supporting electrolyte formulates an amperometric trait in the form of staircase-like configuration, and the regular stepwise amperometric behavior is scrutinized against the enhanced glucose levels (Fig. 7a). The cumulated swift electron transference kinetics at PVdF-HFP/Co–Fe is foreseen from the attainment of a constant amperometric current at 5 s. The interfacial contact of PVdF-HFP/Co–Fe with an analyte is augmented via the open porous scaffolds and elevated accessible surface area of nanofiber membrane, expanding the effectiveness of an analyte exploitation. The intertwined nanofibers of PVdF-HFP/Co–Fe pronounce the persistent

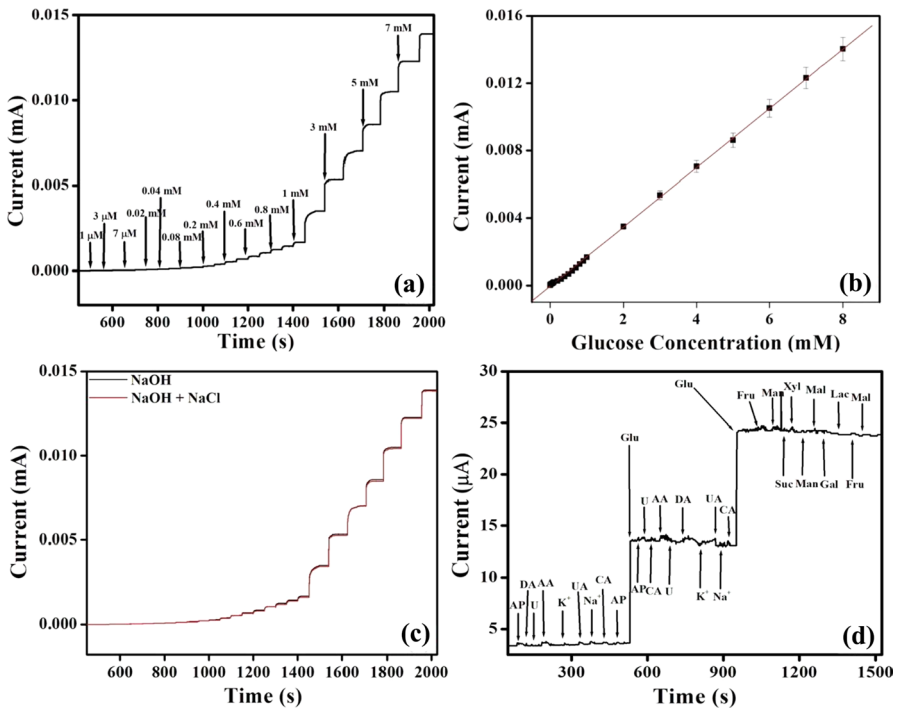


Fig. 7 **a** Amperometric *i-t* retorts of PVdF-HFP/Co-Fe against the dissimilated glucose levels (pH = 13), **b** calibration plot of I_{pa} versus glucose levels, **c** chloride poisoning test in the presence of 0.1 M NaCl, and **d** interfering test of PVdF-HFP/Co-Fe against 8 mM glucose and 0.8 mM interfering species

electron mobility, while the consistent and robust embellishment of metallic nanoparticles on fibers implants the catalytic sites, which jointly enumerates the electrically conductive, catalytically active, and robust electrochemical sites. Thus, the reinforced electron mobility channels, extended porosity, bimetallic synergism, and uniform active sites of PVdF-HFP/Co-Fe confine the interfacial resistance and accelerate the glucose-sensing features. PVdF-HFP/Co-Fe demonstrates a good linearity for a broad glucose levels of 0.001 to 8 mM, and the detection limit and sensitivity, respectively, of 0.65 M and $375.01 \mu\text{A mM}^{-1} \text{cm}^{-2}$ are visualized from the respective linear fit (Fig. 7b) [40]. Customarily, the utilization potential of as-formulated electrochemical probes in glucose diagnosis kits is restrained with the predominant impediments of traditional electrodes such as strenuous polishing and pre-treatment, surface alteration of electrodes with catalytic slurry, exploitation of an insulating binder, elevated resistance, metallic sites' percolation from electrode surface, inferior endurance, and raised expenditure. The above imperfections of accustomed electrochemical probes are proficiently confronted with the in situ development of Co-Fe nanoparticles on PVdF-HFP fibers (PVdF-HFP/Co-Fe). Despite the inferior glucose detection sensitivity of PVdF-HFP/Co-Fe over few reports, the profitable configurations

including affordable, repeatable, and easier manufacturing and sensing processes endorse the adequate applicability of PVdF-HFP/Co-Fe in ELEGSSs. Thus, the PVdF-HFP/Co-Fe's ELEGSS performance along with the above supremacies out-fits the similarly configured earlier glucose-sensing reports (Table S1). The post-mortem SEM analysis of PVdF-HFP/Co-Fe membrane reveals that the significant morphological entities of both the fiber and Co-Fe nanoparticles endure indistinguishable from that of pristine PVdF-HFP/Co-Fe membrane, elucidating the morphological integrity of as-formulated membrane.

The catalytic activity loss of metal nanoparticles under Cl^- ions environment is pronounced through the metal-Cl configuration [41]. The inescapable circumstances of analyte's acquaintance with Cl^- ions impulse the consideration of Cl^- poisoning effect for the fabricated ELEGSSs. Accordingly, PVdF-HFP/Co-Fe's amperometric *i-t* test was perceived with glucose in 0.1 M NaCl (pH=13) (Fig. 7c). The invariable amperometric trait scrutinized between the lack and existence of Cl^- ions confirms the exceptional anti- Cl^- poisoning possession of PVdF-HFP/Co-Fe membrane.

Interference studies

As the supremacy of ELEGSSs is liable on the discernment of electrode's intervention species [42], the anti-intervening ability of PVdF-HFP/Co-Fe was scrutinized with the *i-t* performance against the sequential instillations of 8 mM glucose at variant junctures, consequential with the interfering molecules (pH=13) at 0.5 V versus Ag/AgCl (Fig. 7d). Apprehensible oxidation retort was not visualized against the interferences including AP, DA, U, AA, K^+ , UA, Na^+ , and CA, while the noteworthy behavior is illustrated for an interest of analyte-glucose. Compared to the glucose, the electron conveyance proportions of UA and AA are noticeably higher under their lower concentrations. Conversely, the insignificant *i-t* retorts assimilated for PVdF-HFP/Co-Fe endorse its high specificity on glucose detection. The specific applied potential of 0.5 V versus Ag/AgCl and robust specificity of Co-Fe consequence the nullified interference retorts of PVdF-HFP/Co-Fe [43, 44]. Additionally, PVdF-HFP/Co-Fe's retort against the common mono/disaccharides augments its excellent specificity toward glucose oxidation. It is also noted that the pre-accumulation of interferences do not negatively influence the glucose diagnosis, widening the selective glucose diagnosis amid the existence of other intervening species.

Electrochemical glucose-sensing studies for scale-up processes

PVdF-HFP/Co-Fe's electrocatalytic stability toward glucose diagnosis is actualized using amperometric *i-t* test in 5 mM glucose/0.1 M NaOH at 0.5 V versus Ag/AgCl. PVdF-HFP/Co-Fe establishes the vigorous electrocatalytic stability on glucose diagnosis as enunciated from the preservation of 93.2% current response at 60th day from its initial response (Fig. S3). PVdF-HFP/Co-Fe reveals a relative standard deviation (RSD) of 2.9% for 11 *i-t* assessments with a solitary probe, stating the

Table 1 ELEGs performance of PVdF-HFP/Co–Fe membrane in human serum

Glucose concentration		Glucose added (μM)	Glucose found (mM)		RSD (%)	Recovery (%)
Original serum (mM)	Diluted serum (mM)		Accu-Chek glucometer	Proposed method		
9.6	4.0	0	3.91	3.93	2.12	98.3
		100	4.12	4.09	2.34	99.8
		200	4.24	4.21	2.56	100.2
		300	4.32	4.39	2.63	102.1
		400	4.42	4.55	2.25	103.4

tremendous repeatability of as-formulated membrane. 3.4% RSD accrued for PVdF-HFP/Co–Fe membrane enunciates the reproducibility of a processed probe.

Real sample analysis

The affluence of as-formulated catalytic probe in ELEGs is accentuated only with its performance in physiological sample [45]; accordingly, PVdF-HFP/Co–Fe's glucose detection in practical fragment was perused in human serum. The pre-anticipated concentrations of an interest of analyte were instilled into the lessened concentration of human serum, and PVdF-HFP/Co–Fe's behavior against the above glucose levels was electrochemically investigated using an amperometric approach at 0.5 V versus Ag/AgCl. The sizeable recovery (98.3–103.4%) and RSD (2.12–2.63) established for PVdF-HFP/Co–Fe on glucose detection (Table 1) are in line with the marketized glucometer's results, articulating the as-formulated nanofiber membrane's scale-up capability.

Conclusions

The orderly implanted metallic active channels on electrospun nanofiber membranes are accomplished with the aid of a chemical reduction strategy. The elongated porous nature of fiber membranes serves as a reservoir for the storage of glucose, and the analyte's intimate contact with active sites accelerates the electrode/electrolyte interfacial properties. The high specificity of as-formulated PVdF-HFP/Co–Fe on glucose sensing is authenticated under the actuality of interference species. PVdF-HFP/Co–Fe's realism in glucose recognition is manifested with the substantial recovery rates in human serum, which is in par with the marketized glucometer. Thus, the conversion of an insulating and inert host material, respectively, into electron conductive and electrochemically active probe constructs the efficient ELEGs performance, which directs the first-hand archetypes to manufacturing the time- and cost-efficient glucose sensors.

Supplementary Information The online version contains supplementary material available at <https://doi.org/10.1007/s11164-021-04553-0>.

Acknowledgements This research effort was supported by the Department of Science and Technology (DST), New Delhi, Major Project Grant No.: DST/TMD/HFC/2K18/52(C). The authors are thankful to the Deanship of Scientific Research at King Khalid University for funding this work through the Research Group Project under Grant number R.G.P.2/96/42.

Declarations

Conflict of interest The authors declare that they have no conflict of interest.

Ethical approval This article does not contain any studies with human or animal subjects.

Informed consent A statement regarding informed consent is not applicable.

References

1. D. Soumya, B. Srilatha, J. Diabetes Metab. **2**, 1000167 (2011)
2. I.B. Hirsch, D. Armstrong, R.M. Bergenstal, B. Buckingham, B.P. Childs, W.L. Clarke, A. Peters, H. Wolpert, Diabetes Technol. Ther. **10**, 232 (2008)
3. X. Niu, X. Li, J. Pan, Y. He, F. Qiu, Y. Yan, RSC Adv. **6**, 84893 (2016)
4. Q. Wang, Q. Wang, K. Qi, T. Xue, C. Liu, W. Zheng, X. Cui, Anal. Methods **7**, 8605 (2015)
5. A. Esmaeeli, A. Ghaffarinejad, A. Zahedi, O. Vahidi, Sens. Actuators B Chem. **266**, 294 (2018)
6. P. Sivasakthi, G.N.K. Ramesh Bapu, M. Chandrasekaran, Mater. Sci. Eng. C **58**, 782 (2016)
7. A. Weremfo, S.T.C. Fong, A. Khan, D.B. Hibbert, C. Zhao, Electrochim. Acta **231**, 20 (2017)
8. F. Yang, J. Liu, Z. Lu, P. Dai, T. Nakamura, S. Wang, L. Chen, A. Wakamiya, K. Matsuda, Adv. Sci. **7**, 1902474 (2020)
9. W. Xu, S. Dai, X. Wang, X. He, M. Wang, Y. Xi, C. Hu, J. Mater. Chem. B **3**, 5777 (2015)
10. H. Liu, X. Wu, B. Yang, Z. Li, L. Lei, X. Zhang, Electrochim. Acta **174**, 745 (2015)
11. S. Mondal, R. Madhuri, P.K. Sharma, J. Mater. Chem. C **5**, 6497 (2017)
12. Y. Mu, D. Jia, Y. He, Y. Miao, H.L. Wu, Biosens. Bioelectron. **26**, 2948 (2011)
13. S. Tanaka, Y.V. Kaneti, R. Bhattacharjee, M.N. Islam, R. Nakahata, N. Abdullah, S. Yusa, N.-T. Nguyen, M.J.A. Shiddiky, Y. Yamauchi, M.S.A. Hossain, A.C.S. Appl. Mater. Interfaces **10**, 1039 (2018)
14. T.N.H. Nguyen, X. Jin, J.K. Nolan, J. Xu, K.V.H. Le, S. Lam, Y. Wang, M.A. Alam, H. Lee, A.C.S. Biomater. Sci. Eng. **6**(9), 5315 (2020)
15. F. Amri, N.L.W. Septiani, M. Rezki, M. Iqbal, Y. Yamauchi, D. Golberg, Y.V. Kaneti, B. Yulianto, J. Mater. Chem. B **9**, 1189 (2021)
16. H. Xu, F. Han, C. Xia, S. Zhuikov, G. Zheng, Electrochim. Acta **331**, 135295 (2020)
17. T. Maiyalagan, C. Mahendiran, K. Chaitanya, R. Tyagi, F.N. Khan, Res. Chem. Intermed. **38**(2), 383 (2012)
18. G.G. Kumar, J. Mater. Chem. **21**(43), 17382 (2011)
19. T.R. Kumar, K.J. Babu, D.J. Yoo, A.R. Kim, G.G. Kumar, RSC Adv. **5**, 41457 (2015)
20. A.B. Rinkevich, D.V. Perov, M.I. Samoilovich, S.M. Klescheva, Metamaterials **6**, 27 (2012)
21. T. Wang, Y. Yu, H. Tian, J. Hu, Electroanalysis **26**, 2693 (2014)
22. T. Mudrinić, S. Marinović, A.M. Nikolić, N.J. Jovičić, M. Ajduković, Z. Mojović, P. Banković, Sens. Actuators B Chem. **299**, 126976 (2019)
23. M. Li, P. Dong, Y. Zhang, J. Alloys Compd. **810**, 151927 (2019)
24. N. Senthilkumar, K.J. Babu, G.G. Kumar, A.R. Kim, D.J. Yoo, Ind. Eng. Chem. Res. **53**, 10347 (2014)
25. Y. Ding, P. Zhang, Z. Long, Y. Jiang, F. Xu, W. Di, J. Membr. Sci. **329**, 56 (2009)
26. T. Xu, J. Xue, X. Zhang, G. He, H. Chen, Appl. Surf. Sci. **402**, 294 (2017)

27. J. Xu, Y. Shi, X. Zhang, H. Yuan, B. Li, C. Zhu, X. Zhang, Y. Chen, *J. Mater. Chem. C* **8**, 7847 (2020)
28. K.J. Babu, N. Senthilkumar, A.R. Kim, G.G. Kumar, *Sens. Actuators B Chem.* **241**, 541 (2017)
29. S. Shahabuddin, N.M. Sarih, S. Mohamad, S.N. Atika Baharin, *RSC Adv.* **6**, 43388 (2016)
30. H.A. Zadeh, M.A. Salmasi, *Anal. Bioanal. Chem. Res.* **5**, 23 (2018)
31. L.-M. Cao, Y.-W. Hu, S.-F. Tang, A. Iljin, J.-W. Wang, Z.-M. Zhang, T.-B. Lu, *Adv. Sci.* **5**, 1800949 (2018)
32. A. Glaria, S. Soule, N. Hallali, W.-S. Ojo, M. Mirjolet, G. Fuks, A. Cornejo, J. Allouche, J.C. Dupin, H. Martinez, J. Carrey, B. Chaudret, F. Delpech, S. Lachaize, C. Nayral, *RSC Adv.* **8**, 32146 (2018)
33. F. Qiu, L. Li, G. Liu, Y. Wang, Y. Wang, C. An, Y. Xu, C. Xu, Y. Wang, L. Jiao, H. Yuan, *Int. J. Hydrog. Energy* **38**, 3241 (2013)
34. L.A. Saghatforoush, S. Sanati, M. Hasanzadeh, *Res. Chem. Intermed.* **41**(7), 4361 (2015)
35. R. Sahay, P.S. Kumar, R. Sridhar, J. Sundaramurthy, J. Venugopal, S.G. Mhaisalkar, S. Ramakrishna, *J. Mater. Chem.* **22**, 12953 (2012)
36. J. Huang, Y. Liao, G. Li, N. Xu, M. Xu, W. Li, *Electrochim. Acta* **299**, 45 (2019)
37. J. Wang, Y. Liu, L. Cheng, R. Chen, H. Ni, J. Alloys Compd. **821**, 153510 (2020)
38. R.S. Kumar, K. Govindan, S. Ramakrishnan, A.R. Kim, J.-S. Kim, D.J. Yoo, *Appl. Surf. Sci.* **556**, 149765 (2021)
39. P.P. Bardapurkar, S.S. Shewale, S.A. Arote, S.S. Pansambal, N.P. Barde, *Res. Chem. Intermed.* **47**(5), 1919 (2021)
40. K.E. Toghill, R.G. Compton, *Int. J. Electrochem. Sci.* **5**, 1246 (2010)
41. A. Glaria, S. Soule, N. Hallali, W.S. Ojo, M. Mirjolet, G. Fuks, A. Cornejo, J. Allouche, J.C. Dupin, H. Martinez, J. Carrey, B. Chaudret, F. Delpech, S. Lachaize, C. Nayral, *RSC Adv.* **8**, 32146 (2018)
42. D. Aayed, E. Laubender, M. Souiri, O. Yurchenko, H. Marmouch, G. Urban, A. Othmane, *J. Electrochem. Soc.* **164**, B767 (2017)
43. Y. Luo, Q. Wang, J. Li, F. Xu, L. Sun, Y. Bu, Y. Zou, H.B. Kraatz, F. Rosei, *Inorg. Chem. Front.* **7**, 1512 (2020)
44. K.J. Babu, T. Rajkumar, D.J. Yoo, P. Siew-Moi, G.G. Kumar, *ACS Sustainable Chem. Eng.* **6**(12), 16982 (2018)
45. K. Vasuki, G. Siva, A. Balasubramani, M. Pannipara, A.G. Al-Sehemi, Y. Xia, R. Fang, D.J. Yoo, T.R. Kumar, R. Ramachandran, G.G. Kumar, *Appl. Phys. A Mater. Sci. Process* **125**, 381 (2019)
46. H. Jia, N. Shang, Y. Feng, H. Ye, J. Zhao, H. Wang, C. Wang, Y. Zhang, *J. Colloid Interface Sci.* **583**, 310 (2021)

Publisher's Note Springer Nature remains neutral with regard to jurisdictional claims in published maps and institutional affiliations.

Authors and Affiliations

J. Saravanan¹ · A. Vignesh¹ · Syed Shaheen Shah² · Md. Abdul Aziz² · Mehboobali Pannipara³ · Abdullah G. Al-Sehemi³ · Siew-Moi Phang^{4,5} · Fong-Lee Ng⁴ · Bakrudeen Ali Ahmed Abdul⁶ · G. Gnana kumar¹ 

¹ Department of Physical Chemistry, School of Chemistry, Madurai Kamaraj University, Madurai 625021, India

² Centre of Research Excellence in Nanotechnology (CENT), King Fahd University of Petroleum and Minerals (KFUPM), Dhahran 31261, Saudi Arabia

³ Department of Chemistry, King Khalid University, Abha 61413, Saudi Arabia

⁴ Institute of Ocean and Earth Sciences (IOES), University of Malaya, 50603 Kuala Lumpur, Malaysia

-
- ⁵ Faculty of Applied Sciences, UCSI University, 56000 Kuala Lumpur, Malaysia
- ⁶ Faculty of Applied Sciences, Ton Duc Thang University, Ho Chi Minh City, Vietnam